Biaxial and antiferroelectric structure of the orthogonal smectic phase of a bent-shaped molecule and helical structure in a chiral mixture system

Sungmin Kang,* Ha Nguyen, Shunpei Nakajima, Masatoshi Tokita, and Junji Watanabe
Department of Organic and Polymeric Materials, Tokyo Institute of Technology, Ookayama, Meguro-ku, Tokyo 152-8442, Japan
(Received 8 January 2013; revised manuscript received 19 February 2013; published 13 May 2013)

We examined the biaxial and antiferroelectric properties in the Smectic-AP_A (Sm-AP_A) phase of bent-shaped DC-S-8. The biaxiality, which results from the existence of a secondary director, was well established from birefringence observations in the homeotropically aligned Sm-AP_A. By entering into Sm-AP_A phase, the birefringence (Δn, difference between two refractive indices of short axes) continuously increased from 0 to 0.02 with decreasing temperature. The antiferroelectric switching and second harmonic generation (SHG) activity on the field-on state were also observed in the Sm-AP_A phase, and the evaluated spontaneous polarization (P_S) value strongly depended on temperature. The temperature dependence of Δn and P_S resembles each other and follows Haller's approximation, showing that the biaxiality is due to polar packing in which the molecules are preferentially packed with their bent direction arranged in the same direction, and that the phase transition of Sm-AP_A to Sm-A is second order. The biaxiality was further examined in chiral Sm-AP_A*. Doping with chiral components induced the helical twisting of the secondary director in the Sm-AP_A* phase, which was confirmed by observing the reflection of the circular dichroism (CD) bands in the homeotropically aligned cell. The helical pitch of Sm-AP_A* is tunable in the range of 300–700 nm wavelength with a variation in the chiral content of 5 to 10 weight (wt)%.

DOI: 10.1103/PhysRevE.87.052501 PACS number(s): 61.30.−v, 78.15.+e, 77.80.−e

I. INTRODUCTION

Bent-core liquid crystals have attracted substantial attention over the past decade due to the spontaneous formation of polar order and chiral structure regardless of whether the constituent molecules are chiral [1,2]. Thus, a vast number of bent-core materials have so far been synthesized and characterized to clarify the structure-properties correlation [3,4]. Most of them form the so-called banana phases designated as B1 to B7. In addition, a particular type of polar smectic phase has attracted attention, the switchable orthogonal smectic phase, which is a candidate for practical applications because of its fast-switching ability due to the polar layer structure [5]. A couple of Sm-AP phases, for example, Sm-A_dP_A [6], Sm-AP_A [7–12], and Sm-AP_F [13] were identified. Subscripts d, A, and F stand for partial bilayer, antiferroelectric, and ferroelectric, respectively. In the homeotropic cells, Sm-AP_A and Sm-AP_F are optically biaxial; in contrast, Sm-A_dP_A is dark and becomes birefringent when an electric field is applied. Several symmetric compounds were synthesized displaying a quite broad temperature range for the Sm-AP_A phase [10,13,14]. In addition, Nagaraj *et al.* recently proposed and demonstrated liquid crystal display (LCD) modes using a quite unique compound with comparatively high contrast ratio and low driving force [15,16]. Furthermore, very recently, Sm-AP_α phase has also been observed between Sm-AP_R and Sm-AP_A phase, which can be explained by Sm-C_α [17].

In this study, we investigated the structural properties of the orthogonal Sm-AP_A phase formed from bent-shaped DC-S-8 [see Fig. 1(a)] [12] by observing the birefringence and spontaneous polarization that are induced by the second polar director. Furthermore, we studied the twisting deformation of the second director in the chiral Sm-AP_A* phase, which forms from chiral mixtures with DC-S-8* and possesses an analogous structure to that of DC-S-8 but contains a chiral center at the flexible alkyl tails [see Fig. 1(b)].

II. EXPERIMENT

We synthesized DC-S-8 and DC-S-8* (*s* isomer) according to the scheme reported in a previous paper [12]. Phase transition temperatures and enthalpies of the mixtures were determined by differential scanning calorimetry (DSC, Perkin Elmer Pyris1) using a rate of 1 °C min^{-1} during heating and cooling. Textural observations were also made by using a polarized optical microscope (POM, Olympus BX50) connected to a hot stage with a temperature controller (Mettler Toledo FP82).

A function generator equipped with a high-speed voltage amplifier was utilized to study the electro-optical switching behavior. The polarization reversal currents were measured across the 1 MΩ resistor by standard triangular or rectangular electric waves. The birefringence dispersion was estimated by fitting the transmittance spectrum obtained with a multichannel fiber spectroscope (USB400, Ocean Photonics) equipped with a polarized optical microscope (Nikon Eclipse LV100POL). In addition, circular dichroism (CD) was measured by using a spectropolarimeter (JASCO J-720WI).

The sandwiched cells in the electro-optical measurements were prepared using glass plates coated with indium tin oxide (ITO). Commercially available polyimide (for vertical alignment usage) was used as the alignment layer for the homeotropic orientation in the cell. An ultraviolet (UV)-curable adhesive mixed with spacer beads was used to get cells with a typical thickness of ∼5 μm. The samples were introduced into the cells by capillary action at the isotropic (I) state.

The second harmonic generation (SHG) was measured by Q-switched Nd:YAG laser light (1064 nm) irradiated

*Corresponding author: skang@polymer.titech.ac.jp

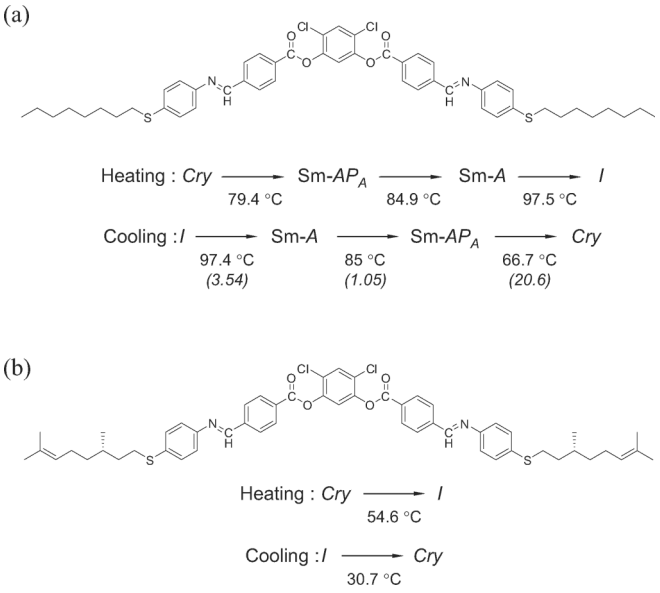

FIG. 1. Structure and phase sequence of (a) DC-S-8 and (b) DC-S-8*. The following abbreviations are used: crystal (*Cry*), isotropic fluid (*I*), nonpolar uniaxial smectic (Sm-*A*) phase, and antiferroelectric and biaxial smectic (Sm-AP_A) phase. Transition enthalpies (kJ mol^{-1}) are given in parenthesis for cooling process.

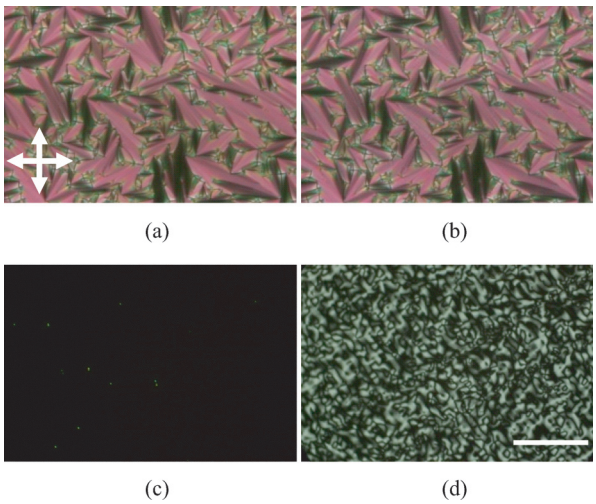

FIG. 2. (Color online) Optical photomicrographs of DC-S-8 observed in various surface-treated ITO sandwich cells at different temperatures: (a) and (b) show the typical fan-shaped textures of Sm-*A* and Sm-AP_A at 90 °C and 80 °C in 5-μm thickness planar cells, respectively. (c) and (d) show the dark and birefringent Schlieren textures of Sm-*A* and Sm-AP_A, respectively, in the homeotropically aligned sample. The scale bar indicates 25 μm.

onto the glass cell sample (illumination area: 0.1 mm in diameter) after passing it through a quarter-wave plate and a polarizer. The generated SH light (532 nm) was detected in the direction of the transmission after passing through an infrared-radiation (IR) cutoff filter, an interference filter, and an analyzer.

III. RESULTS AND DISCUSSION

A. Biaxial nature of the Sm-AP_A phase

The subtle transition from Sm-*A* to Sm-AP_A in DC-S-8 shows an enthalpy change of 1.05 kJ mol^{-1}, which is relatively smaller than that of the isotropic to Sm-*A* transition [see Fig. 1(a)]. The POM textures in Fig. 2 show the well-defined fan-shaped textures of the homogeneously aligned Sm-*A* and Sm-AP_A phases. No significant change takes place during the transformation except for a slight change in the birefringence color. However, in the homeotropically aligned cell, two phases can be clearly distinguished. A completely dark texture was observed in the temperature range of Sm-*A* [see Fig. 2(c)], whereas a Schlieren texture with both four- and two-brush defects could be seen in the Sm-AP_A phase [see Fig. 2(d)]. The x-ray diffraction pattern shows no essential difference between these two phases. In addition, both phases show a broad outer reflection with a spacing of 4.5 Å and an inner reflection with spacing of 43.5 Å. The latter is nearly equal to the molecular length. Thus, the molecules are packed into a layer with liquidlike packing and long axes perpendicular to the layer [12].

The biaxial nature of Sm-AP_A was examined by measuring the birefringence of the homeotropically aligned ITO cells whose thickness is 14.1 μm. An in-plane switching (IPS) electric field was applied across a gap of 25 μm with the field direction tilted by 45° to the cross polarizers. As mentioned before, the Sm-AP_A phase of DC-S-8 displayed a polydomain Schlieren texture in the absence of an electric field [see Figs. 2(d) and 3(a)]. By applying a direct current (DC) voltage, the texture of Sm-AP_A changed to uniform and bright between the electrodes [see Fig. 3(b)] as a result of the unidirectional orientation of the second director.

The transmitted light intensity (I_t) in the homeotropically aligned sample was measured as a function of the wavelength of incident light λ and the birefringence was estimated by

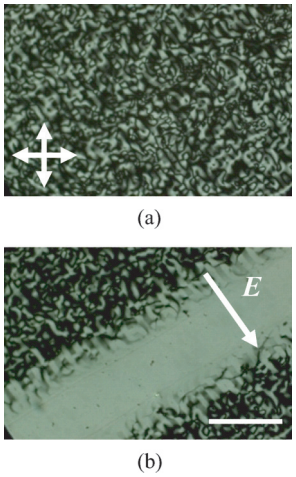

FIG. 3. (Color online) Optical photomicrographs of the DC-S-8 in the vertically aligned cell with a thickness of 4.8 μm upon applying an in-plane DC voltage of 10 V across a gap of 25 μm: (a) polydomain Schlieren texture at the DC-off state and (b) uniform birefringent texture at the DC-on state. The scale bar indicates 25 μm.

using Eq. (1)

$$I_t = I_0 \sin^2(2\theta) \sin^2\left(\frac{\pi d \Delta n}{\lambda}\right). \quad (1)$$

The angle (θ), which is the angle between the direction of the polarization of the incident light and the polarizer, was set at 45° and the intensity strongly depends on the wavelength of the incident light for a constant optical path of d. Figure 4(a) shows the measured intensity of the transmittance light during the DC application (4 V μm^{-1}) on the IPS cell with the homeotropic alignment of pure DC-S-8 in Sm-AP_A [18]. It can be seen that the positions of the intensity maxima of the transmittance curves gradually shift to the long-wavelength region upon cooling, which can be interpreted as an increase

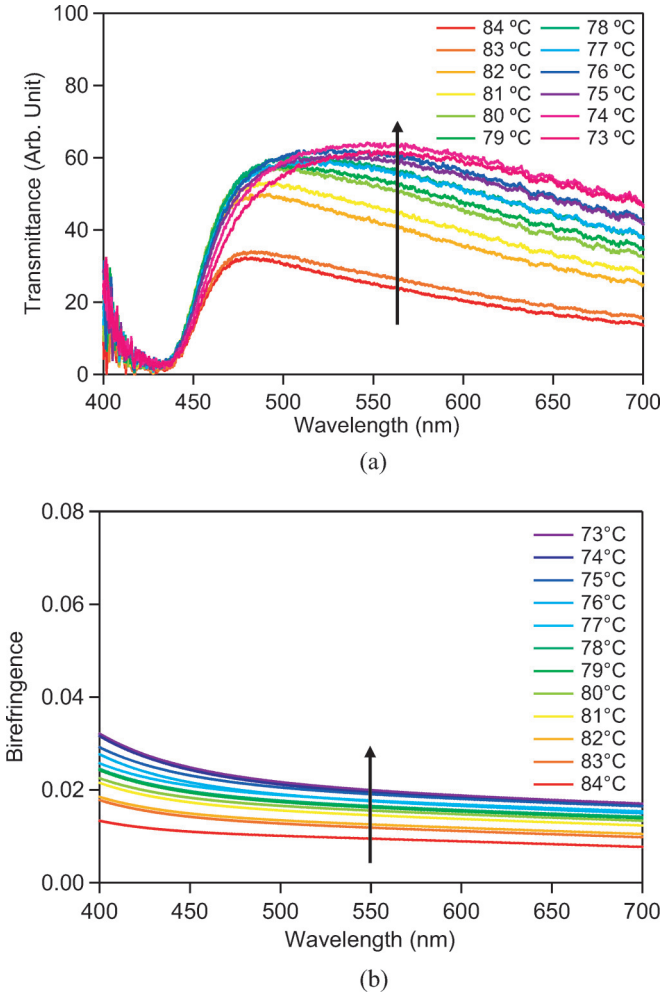

FIG. 4. (Color online) (a) Light transmittance intensity of DC-S-8 as a function of light wavelength at various temperatures measured in the in-plane switching ITO cells with vertical alignment (cell thickness: ~14 μm) by POM equipped with spectrometer. Since the net retardation is too small to precisely determine the birefringence, a wavelength plate (3λ) was used to enlarge the total transmitted retardation [18]. Then, the birefringence was calculated by using equation (1) and (2). (b) Birefringence of DC-S-8 on E_{ON} state (Sm-AP_F) as a function of light wavelength at various temperatures. Due to the absorption band in 400–450 nm, the calculated birefringence value in this region also bears less reliability. The arrow in each figure indicates a direction of temperature decreasing.

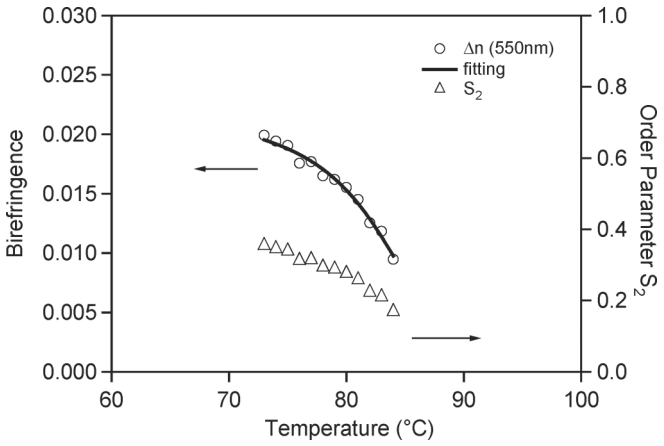

FIG. 5. Temperature dependence of the birefringence ($\mathbf{n_p} - \mathbf{n_o}$) observed by homeotropic alignment and order parameter (S_2) in the Sm-AP_A phase. The order parameter (for 550 nm) was calculated by using Haller's approximation in Eq. (3).

in birefringence. The transmitted light intensity I_t was curve fitted by applying Cauchy's Eq. (2) for Δn in Eq. (1) [19,20]

$$\Delta n(\lambda) = a + \frac{b}{\lambda^2} + \frac{c}{\lambda^4}. \quad (2)$$

By approximating the constants, a, b, and c, the wavelength dependence of Δn was determined as shown in Fig. 4(b). The Δn values collected at 550 nm were plotted against temperature in Fig. 5. The Δn, which is the birefringence of the secondary director [$\mathbf{n_p} - \mathbf{n_o}$, see Fig. 6(a)], clearly increases continuously from 0 to 0.02 with decreasing temperature in the Sm-AP_A temperature region, suggesting a second-order transition between the Sm-A and Sm-AP_A phases. By adopting Haller's approximation in Eq. (3) [21],

$$S_2 (= \Delta n/\Delta n_0) = (1 - T/T^*)^{\beta}, \quad (3)$$

we examined the evolution of the order parameter S_2 (subscript "2" refers to order parameter of secondary director) as a

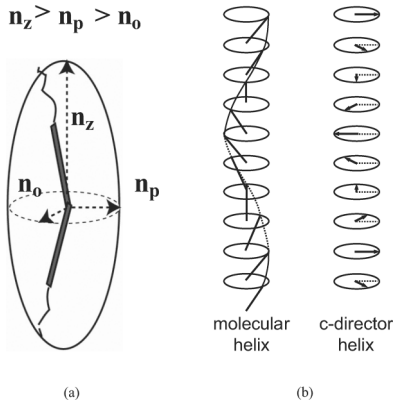

FIG. 6. (a) Refractive index ellipsoid of a bent-core molecule along the primary ($\mathbf{n_z}$) and two secondary ($\mathbf{n_p}$, $\mathbf{n_o}$) directors in each layer of the Sm-AP phase and (b) schematic structure of the helical superstructure in the Sm-AP^* phase, possibly formed from the helical rotation of the two secondary ($\mathbf{n_p}$, $\mathbf{n_o}$) directors perpendicular to the smectic layer as in Sm-C^* and Sm-$C_A{}^*$. In this study, the birefringence refers a difference between two secondary refractive indices ($\mathbf{n_p}$, $\mathbf{n_o}$).

function of temperature (see Fig. 5), where Δn_0 (the birefringence expected for perfect orientation, $S_2 = 1$) equals 0.05, β (the material constant) is 0.346, and T^* (the Sm-A − Sm-AP_A transition temperature) is 84.4 °C. It should be noted that the application of Haller's approximation is usually utilized for an order parameter of primary director; however, we adopt it since we consider the nature of secondary directors in Sm-A (uniaxial) and in Sm-AP_A [biaxial, see Fig. 2(d)] can be thought as isotropic and nematic-like, respectively, in case of homeotropic observations. Thus, here, the higher value of β might be interpreted as indicating an intrinsic property of temperature dependence of birefringence that stems from secondary order parameter, S_2. The order parameter S_2 changes from 0 (for Sm-A) to 0.31 upon cooling, which is quite smaller than the typical value for the primary n director in the nematic phase of the conventional rodlike LC molecules.

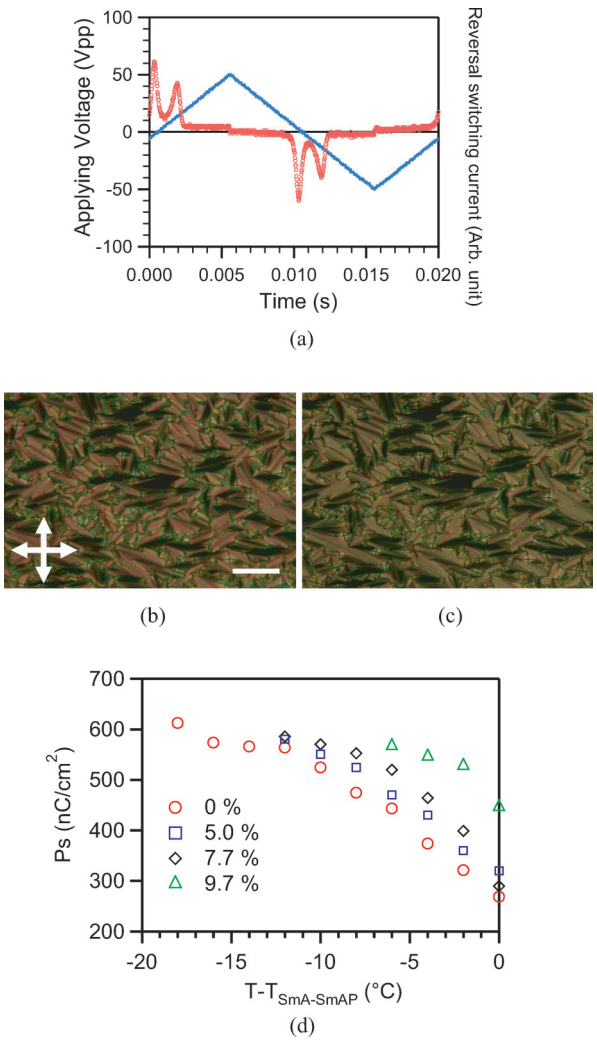

FIG. 7. (Color online) (a) Switching current in the Sm-AP_A* phase recorded at 75 °C in the 6.8-μm thick planar orientation ITO cell. The applied electric field was 100 Vpp (V peak to peak) triangular wave. (b) and (c) Optical photomicrographs before and during the application of the DC electric field. (d) The calculated spontaneous electric polarization of all mixtures from the integration of switching peaks upon applying a triangular electric field (24 Vpp μm^{-1}) as a function of normalized temperature. The arrows indicate the directions of the cross polarizers. The scale bar indicates 50 μm.

B. Polar switching behavior of Sm-AP_A

Biaxiality can be attributed to polar ordering in which the molecules are preferentially packed with their bent direction arranged in the same direction. Figure 7(a) shows the switching current observed in the planar ITO sandwich cell (6.8 μm thickness) using a triangular wave of 50 Hz. Two switching current peaks per half cycle of applied voltage were observed in Sm-AP_A but not in Sm-A. Upon applying the electric field, the weak stripe pattern that previously existed in the fan-shaped domain in the absence of the field instantly disappeared and the birefringence clearly increased. However, the position of the dark extinction brushes parallel to the crossed polarizers and the fan-shaped domains remained unchanged [see Figs. 7(b) and 7(c)], indicating that switching occurs by collective rotation around the molecule's long axis. Spontaneous polarization (P_S) was estimated from the integral of the switching current peak, and P_S continuously increased from 0 upon lowering the temperature and saturated at approximately 600 nC cm^{-2} prior to crystallization as shown in Fig. 7(d). In order to assure polar ordering, SHG was also measured in both the Sm-A and Sm-AP_A phases as a function of temperature with and without an electric field. The collected data are shown in Fig. 8. Upon application of the electric field, the SHG signal could not be detected in the Sm-A phase, but it could be clearly detected in Sm-AP_A with the intensity increasing with decreasing temperature. On field-off, the SHG signal disappeared in the Sm-AP_A phase, showing the antiferroelectric structure of the Sm-AP_A phase.

The temperature dependence of the P_S as well as SHG signal intensity is similar to that of Δn, and it can be followed with Haller's approximation [21]. The value of β and P_{So} were calculated by using Eq. (3) [19,20], which are 0.38 and 2000 nC cm^{-2}, respectively. The similarity in the temperature dependence of Δn and P_S is obvious, because the secondary director denoting the bent direction of the molecules corresponds to the spontaneous polarization axis. Figure 9(a) indicates the possibly second-order-like transition of Sm-A to Sm-AP_A. The decrease of the order parameter in the secondary director could be caused by the gain in rotational freedom around the short axis of the molecule. Thus, as results of

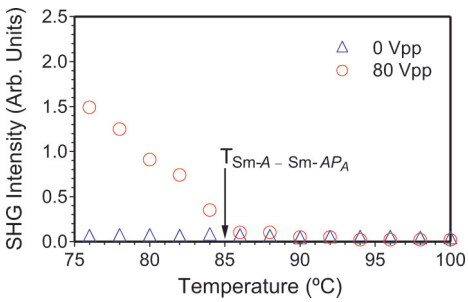

FIG. 8. (Color online) Temperature dependence of the SHG intensity on cooling from the Sm-A to Sm-AP_A phase. Red circles and blue triangles were observed at the electric field-on state and field-off states, respectively. The arrow indicates the transition temperature of Sm-A to Sm-AP_A upon cooling.

birefringence and switching experiments, both temperature dependences of Δn and P_S can be derived from an increase of long-range order of the secondary director by decreasing temperature in the Sm-AP_A phase, as shown in Fig. 10.

C. Chiral Sm-AP_A phase in the binary mixture

Chirality is well known to modify the self-assembly and physical properties of liquid crystals [22–24], which has led to a plethora of studies on chiral liquid crystals. Generally, most of the chiral liquid crystals tend to generate macroscopic helical superstructures, i.e., chiral nematic (N^*) phases and polar switching chiral smectic (Sm-C^*) phases. The well-studied helical structure in Sm-C^* is induced by the rotation of the secondary c director produced by the molecular tilt between adjacent layers as shown in Fig. 6(b). Alternatively, it is the natural biaxiality of Sm-C^* that most contributes to the formation of the helical superstructure [25,26]. Therefore, the question arises whether chirality produces the helical structure in the biaxial Sm-AP_A phase in spite of not having a molecular tilt.

It is common to introduce chirality to bent-core materials by utilizing the asymmetric centers in the tails [27–30] or blending with chiral dopants [31,32]. The former sometimes can lead to the replacement or elimination of the mesophases depending on the materials [32], whereas the latter does not affect the original mesomorphic behavior but modifies it with the appearance of the helical structure as small amounts of dopants are introduced [29,31]. Therefore, the chiral homologue DC-S-8* [Fig. 1(b)] was mixed with DC-S-8 of chiral component content of 3.5, 5.0, 7.7, and 9.7 wt%. Although DC-S-8* forms no liquid crystals, the mixtures with DC-S-8 up to 10 wt% show two chiral Sm-A^* and Sm-AP_A^* mesophases like the pure DC-S-8. Cooling DSC thermograms are shown in Fig. 9(a) and the phase behavior is shown against the chiral content in Fig. 9(b). The I – Sm-A^* and Sm-A^* – Sm-AP_A^* transition temperatures gradually decrease with increasing chiral content, whereas the crystallization temperature is not significantly affected. Thus, the temperature range of the Sm-A^* phase did not change (approximate change of 12 °C), but that of the Sm-AP_A^* became narrower with increasing content of chiral dopant.

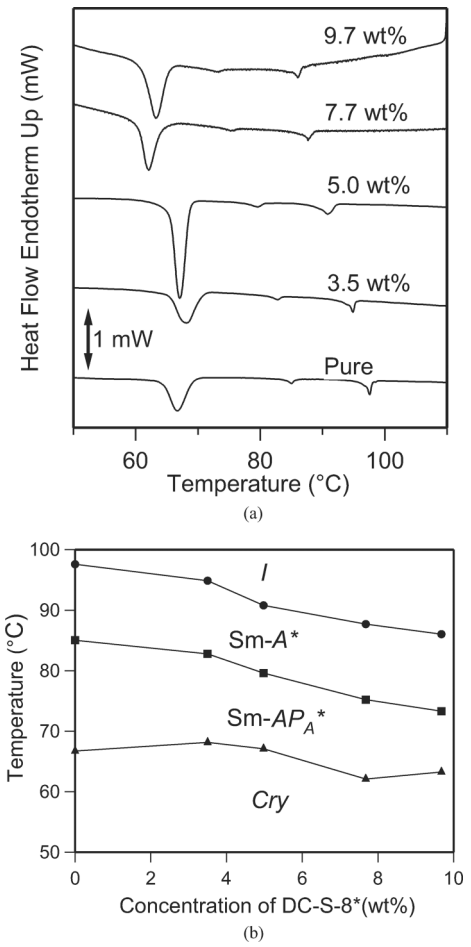

FIG. 9. (a) DSC thermograms of the binary mixtures with DC-S-8* content of 0 to 9.7 wt% and (b) phase transition behavior as a function of chiral content.

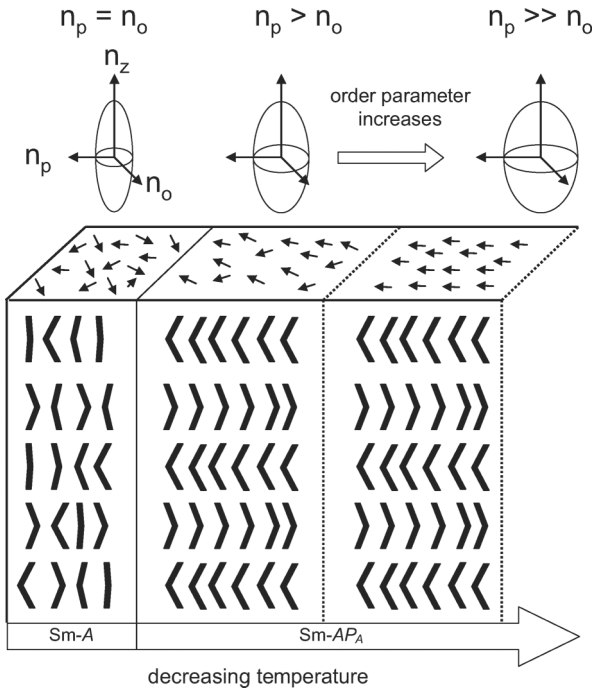

FIG. 10. Schematic illustration of the change in molecular alignment that results in birefringence ($\mathbf{n_p} - \mathbf{n_o}$) change for observation in homeotropically aligned cell during cooling process in Sm-A to Sm-AP_A regime.

The observed textures of all the chiral-doped mixtures were different from that of pure DC-S-8. For instance, upon cooling from the isotropic state of 5.0 wt%, the typical texture of the conventional calamitic Sm-A phase with the fan-shaped domain was obtained [see Fig. 11(a)]. However, upon further cooling into Sm-AP_A^*, the fan-shaped texture did not change but stripes appeared across the fan-shaped texture [see Fig. 11(b)]. This indicates that a structural transformation occurs in the low-temperature mesophase (Sm-AP_A^*) along the layer normal direction. Moreover, as shown in Figs. 11(c) and 11(d), the homeotropically aligned sample of the mixture shows no birefringence for both Sm-A^* and Sm-AP_A^* phases, implying intrinsic optical uniaxiality for both Sm-A^* and Sm-AP_A^*. The situation is same for mixtures with 5.0, 7.7, and 9.7 wt%.

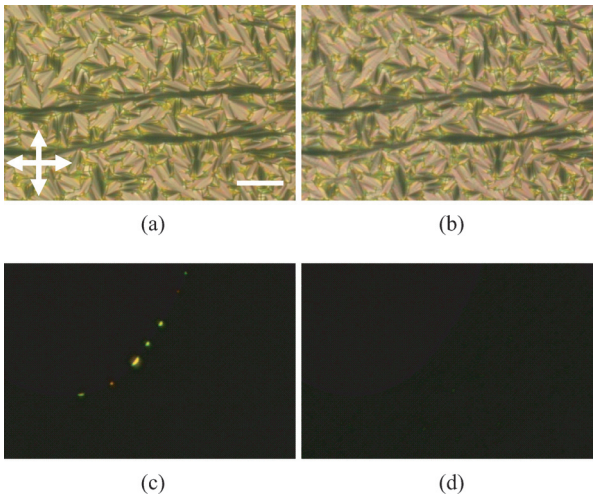

FIG. 11. (Color online) (a)–(d) Optical photomicrographs of the 5.0 wt% mixture (DC-S-8:DC-S-8* = 95:5) observed in the homogeneous and homeotropic aligned surface treated with the ITO sandwich cells at different temperatures: (a) and (b) typical fan-shaped textures of Sm-A^* and Sm-AP_A^* at 86 °C and 77 °C in 5.1 μm thickness planar cells, respectively. (c) and (d) Nonbirefringent textures of the Sm-A^* and Sm-AP_A^* phase in the homeotropically aligned cell with a thickness of 5 μm. The arrows indicate the direction of the cross-polarizers. The scale bar indicates 50 μm.

The absence of birefringence in the homeotropically aligned cell of Sm-AP_A^* implies the helical alignment of the second director. In order to confirm the induced chirality by doping, CD measurements were conducted in 5-μm thick homeotropically aligned samples. Figure 12 shows the CD spectra observed upon cooling from the isotropic state at a rate of 2 °C min^{-1}. No CD signal was detected in the uniaxial Sm-A^* phase; however, on entering the Sm-AP_A^* phase, positive CD bands emerged at wavelength of 635, 420, and 330 nm for mixtures with 3.5, 5.0, and 7.7 wt% chiral content, respectively. The intensity of the CD bands gradually increased with decreasing temperature, without changing the peak wavelength.

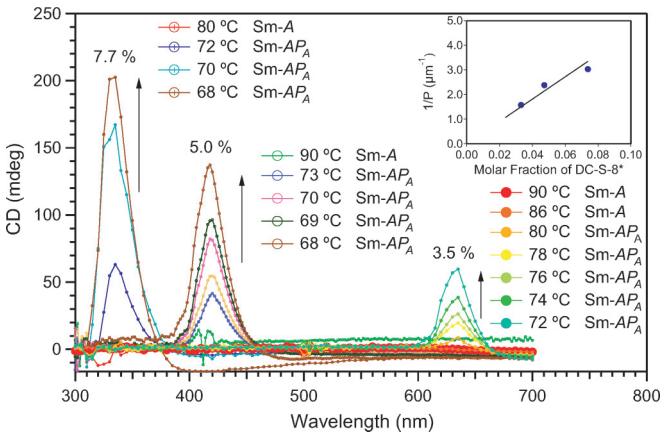

FIG. 12. (Color online) CD reflection bands observed in the homeotropically aligned Sm-AP_A^* phases of chiral mixtures on cooling from the isotropic state at a scanning rate of 2 °C min^{-1}. Reflection bands were observed upon the transformation of Sm-A^* to Sm-AP_A^* with increasing its intensity by decreasing temperature (the arrow in each chiral content indicates the change of direction by temperature decreasing). It is obvious the selective reflection bands decreased with increasing chiral content. The inset indicates the chiral content dependence of the helical twisting power, 1/P.

The CD bands are obviously due to the selective reflection that results from the helical alignment of the secondary director with the helical axis lying parallel to the normal layer. The very weak but sharp reflection bands are due to the low birefringence, and the strong temperature dependence of the intensity reflects the same trend in birefringence. The positive sign of the CD bands for the *S* enantiomer indicates a left-handed helix. From the dependence of the maximum wavelength on the chiral content (see the inset of Fig. 12), the helical twisting power (HTP) value of DC-S-8* was determined around 45 μm^{-1}, which is appreciably large. Only for chiral dopant content of 3.5–7.7 wt%, the twisting angle between the adjacent layers is in the range of 3.7–6.9°, which is calculated by the layer thickness of DC-S-8 as 43.5 Å and the maximum wavelength of the reflection band that corresponds to the half pitch (P).

The polar-reversible switching current is invariably observed in these chiral systems, giving compelling evidence for the antiferroelectric nature of the Sm-AP_A^* phase. The electric field also acts as an external force to unwind the helical structure, i.e., orients the second director toward the electric field. Under crossed polarizers, the dark texture becomes bright. A similar temperature dependence of the P_S and the induced birefringence in the chiral mixtures is also observed as in the DC-S-8.

On turning off the field, the bright texture becomes immediately dark because the intrinsic helical structure is reformed. This in-plane switching behavior can be applied to a light shutter device. One can imagine a ferroelectric/antiferroelectric Sm-C^* phase that leads to fast-switching behavior as compared with the Sm-AP_A^* phase. However, it differs in the sense that the orthogonal Sm-AP_A^* phase is not tilted in the layer that does not form the chevron defect. We believe this switchable phase is a promising candidate for various applications and our study provides valuable information to utilize the intrinsic properties of the biaxial, switchable Sm-AP_A^* phase.

IV. CONCLUSION

In the antiferroelectric Sm-AP_A phase of bent-shaped DC-S-8, the birefringence was well estimated in a homeotropically aligned cell. In the preceding Sm-A phase, the birefringence continuously increased from 0 to 0.02 with decreasing temperature. The antiferroelectricity was also confirmed from observations of the two switching current peaks per half cycle of the triangular voltage and SHG intensity on the field-on state. The P_S strongly depended on temperature as the birefringence. Both the P_S and birefringence temperature dependence superimpose each other, with the data points falling on the curve calculated according to Haller's approximation. This suggests that the Sm-AP_A to Sm-A phase transition is of second order. In other words, the molecules are packed with their bent direction arranged in the same direction within a layer that continuously gains rotational freedom around the molecule's short axis with increasing temperature up to the Sm-A phase.

Doping with chiral components produces the helical structure in the biaxial Sm-$AP_A{}^*$ phase, but not in the uniaxial Sm-A^* phase. Well-defined reflection CD bands were detected in the homeotropically aligned cell, showing that the helical structure was caused by the secondary director. The helical pitch of Sm-$AP_A{}^*$ was tunable within the wavelength range of 300–700 nm as the chiral content varied from 5 to 10 wt%.

We believe current observations of remarkable temperature dependences in birefringence, spontaneous polarization, and intensity of selective reflection CD band in the Sm-AP_A and Sm-$AP_A{}^*$ indicates the biaxiality driven by the secondary director and its critical temperature dependence, which can be interpreted as a thermal fluctuation of order parameter of secondary director in the orthogonal smectic phase.

[1] J. Thisayukta, Y. Nakayama, S. Kawauchi, H. Takezoe, and J. Watanabe, J. Am. Chem. Soc. **122**, 7441 (2000).

[2] T. Niori, T. Sekine, J. Watanabe, T. Furukawa, and H. Takezoe, J. Mater. Chem. **6**, 1231 (1996).

[3] H. Takezoe and Y. Takanishi, Jpn. J. Appl. Phys. **45**, 597 (2006).

[4] R. Amaranatha Reddy and C. Tschierske, J. Mater. Chem. **16**, 907 (2006).

[5] J. Etxebarria and M. B. Ros, J. Mater. Chem. **18**, 2919 (2008).

[6] K. Sadashiva, R. A. Reddy, R. Pratibha, and N. V. Madhusudana, J. Mater. Chem. **12**, 943 (2002).

[7] A. Eremin, S. Diele, G. Pelzl, H. Nadasi, W. Weissflog, J. Salfetnikova, and H. Kresse, Phys. Rev. E **64**, 051707 (2001).

[8] T. Izumi, T. Niori, Y. Simbo, Y. Taknishi, H. Takezoe, and J. Watanabe, J. Phys. Chem. B **110**, 23911 (2006).

[9] S. K. Lee, X. D. Li, S. Kang, M. Tokita, and J. Watanabe, J. Mater. Chem. **19**, 4517 (2009).

[10] C. Keith, M. Prehm, Y. P. Panarin, J. K. Vij, and C. Tschierske, Chem. Commun. **46**, 3702 (2010).

[11] K. Gomola, L. Guo, E. Gorecka, D. Pociecha, J. Mieczkowski, K. Ishikawa, and H. Takezoe, Chem. Commun. **45**, 6592 (2009).

[12] H. Nguyen, S. Kang, M. Tokita, and J. Watanabe, Jpn. J. Appl. Phys. **50**, 071602 (2011).

[13] R. A. Reddy, C. Zhu, R. Shao, E. Korblova, T. Gong, Y. Shen, E. Garcia, M. A. Glaser, J. E. Maclennan, D. M. Walba, and N. A. Clark, Science **332**, 72 (2011).

[14] L. Guo, K. Gomola, E. Gorecka, D. Pociecha, S. Dhara, F. Araoka, K. Ishikawa, and H. Takezoe, Soft Matter **7**, 2895 (2011).

[15] Y. P. Panarin, M. Nagaraj, J. K. Vij, C. Keith, and C. Tschierske, Europhys. Lett. **92**, 26002 (2010).

[16] M. Nagaraj, J. K. Vij, C. Keith, and C. Tschierske, Appl. Phys. Lett. **97**, 213505 (2010).

[17] Y. P. Panarin, M. Nagaraj, S. Sreenilayam, J. K. Vij, A. Lehmann, and C. Tschierske, Phys. Rev. Lett. **107**, 247801 (2011).

[18] See Supplemental Material at http://link.aps.org/supplemental/10.1103/PhysRevE.87.052501 for the UV–vis absorption spectra and the light transmittance intensity of DC-S-8.

[19] Y. Arakawa, S. Nakajima, S. Kang, G. Konishi, and J. Watanabe, J. Mater. Chem. **22**, 14346 (2012).

[20] Y. Arakawa, S. Nakajima, S. Kang, M. Shigeta, G. Konishi, and J. Watanabe, J. Mater. Chem. **22**, 13908 (2012).

[21] I. Haller, Prog. Solid State Chem. **10**, 103 (1975).

[22] H.-S. Kitzerow and C. Bahr, *Chirality in Liquid Crystals* (Springer-Verlag, NewYork, 2001).

[23] R. Lemineux, Chem. Soc. Rev. **36**, 2033 (2007).

[24] C. Tschierske, in *Chirality at the Nano Scale*, edited by D. B. Amabiliino (Wiley-VCH, Weinheim, 2009), p. 271.

[25] W. Helfrich and C. S. Oh, Mol. Cryst. Liq. Cryst. **14**, 289 (1971).

[26] W. Urbach and J. Billard, C. R. Acad. Sci., Paris **274**, 1287 (1972).

[27] I. Nishiyama, J. Yamamoto, and H. Yokoyama, Mol. Cryst. Liq. Cryst. **498**, 19 (2009).

[28] I. Nishiyama, J. Yamamoto, J. W. Goodby, and H. Yokoyama, Mol. Cryst. Liq. Cryst. **443**, 25 (2005).

[29] K. Kumazawa, M. Nakata, F. Araoka, Y. Takanishi, K. Ishikawa,J. Watanabe, and H. Takezoe, J. Mater. Chem. **14**, 157 (2004).

[30] S. K. Lee, S. Heo, J. G. Lee, K. T. Kang, K. Kumazawa, K. Nishida, Y. Shimbo, Y. Takanishi, J. Watanabe, T. Doi, T. Takahashi, and H. Takezoe, J. Am. Chem. Soc. **127**, 11086 (2005).

[31] S. Taushanoff, K. V. Le, J. Williams, R. J. Twieg, B. K. Sadashiva, H. Takezoe, and A. Jakli, J. Mater. Chem. **20**, 5893 (2010).

[32] K. V. Le, S. Aya, Y. Sasaki, H. Choi, F. Araoka, K. Ema, J. Mieczkowski, A. Jakli, K. Ishikawa, and H. Takezoe, J. Mater. Chem. **21**, 2855 (2011).